ACS Photonics

Open Access

pubs.acs.org/journal/apchd5

Article

High Efficiency of Exciton-Polariton Lasing in a 2D Multilayer Structure

Yuening Fan,[¶] Qiaochu Wan,[¶] Qi Yao, Xingzhou Chen, Yuanjun Guan, Hassan Alnatah, Daniel Vaz, Jonathan Beaumariage, Kenji Watanabe, Takashi Taniguchi, Jian Wu,* Zheng Sun,* and David Snoke*

Cite This: *ACS Photonics* 2024, 11, 2722−2728

Read Online

ACCESS | Metrics & More | Article Recommendations | Supporting Information

ABSTRACT: We have placed a van der Waals homostructure, formed by stacking three two-dimensional layers of WS_2 separated by insulating hBN, similar to a multiple-quantum well structure, inside a microcavity, which facilitates the formation of quasiparticles known as exciton-polaritons. The polaritons are a combination of light and matter, allowing laser emission to be enhanced by nonlinear scattering, as seen in prior polariton lasers. In the experiments reported here, we have observed laser emission with an ultralow threshold. The threshold was approximately 59 nW/μm^2, with a lasing efficiency of 3.82%. These findings suggest a potential for efficient laser operations using such homostructures.

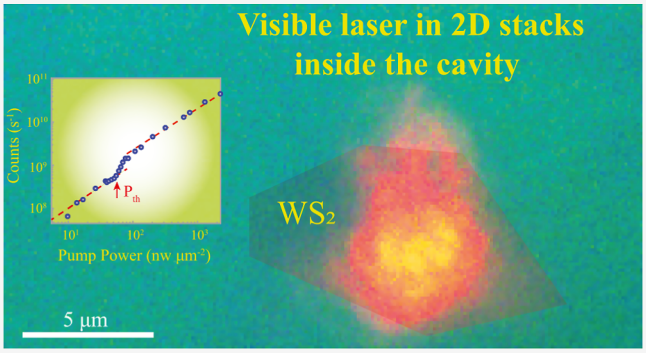

KEYWORDS: *polaritons, transition metal dichalcogenides, microcavities, Bose condensation, lasing*

INTRODUCTION

Nanolasers that employ two-dimensional (2D) materials, particularly transition metal dichalcogenides (TMDs), are gaining significant interest in the field of photonic and optoelectronic devices.[1−4] The inherent properties of 2D TMDs, namely, direct bandgaps and large exciton binding energies, make them ideal for diverse optical applications.[5]

Here, we report a polariton laser using multiple TMD monolayers, with an ultralow lasing threshold and a high efficiency, allowing light emission visible to the naked eye. Exciton-polaritons emerge from the interplay between photons and excitons in semiconductors,[6] with unique benefits.[7] Lasing based on exciton-polaritons can be viewed as a type of Bose−Einstein condensation, a phenomenon that can occur even in the upper branch of the polariton spectrum.[8] As discussed in previous works,[9,10] the nonlinear properties of polariton lasers lead to the enhancement of carrier scattering into lasing states. This gives rise to the possibility of achieving a significantly lower lasing threshold. The compact nature of these polariton lasers, combined with their short lifetime, could also potentially lead to faster response times.[11] Polariton lasers can be crafted from a variety of substances, such as CdTe, GaAs, ZnO, organics, perovskites, and metallic plasmons.[12−18] However, TMD semiconductors stand out for their strong light−matter interaction[19] and ease of integration into small-scale photonic systems.[20,21] TMDs have been used with high optical gain[22] and tunability[23−26] in compact lasing applications and in a range of optoelectronic devices such as photodetectors, LEDs, and solar cells.[27−29]

Laser efficiency is pivotal as it significantly influences the device's usability, economic feasibility, and application breadth. A recent study claimed an ultralow polariton condensation threshold for exciton-polariton lasers,[30] although a definite measurement of the lasing threshold and the lasing efficiency was not reported. In the work reported here, we have been able to directly measure an ultralow threshold and the lasing efficiency of a multilayer TMD structure. This laser utilizes three monolayers of WS_2 as the gain medium. Between each monolayer, there is a thin-film layer of hBN that is approximately 6 nm thick. This set of layers is effectively the same as a multiple-quantum well (MQW) structure and is encapsulated within top and bottom hBN spacer layers and embedded in a microcavity. The benefits of multiple gain layers have been well established in studies with III−V semiconductor structures since 1995.[31] Increasing the number of gain layers N will both increase the oscillator strength, proportional to N, and raise the saturation density, which linearly scales with N.[9,32] In addition, the increase in the oscillator strength of 2D materials with an increasing number of layers has been measured experimentally.[33]

Our structure has a vertical-cavity surface-emitting laser (VCSEL) geometry, which allows for easy access to the light

Received: March 25, 2024
Revised: June 10, 2024
Accepted: June 11, 2024
Published: June 25, 2024

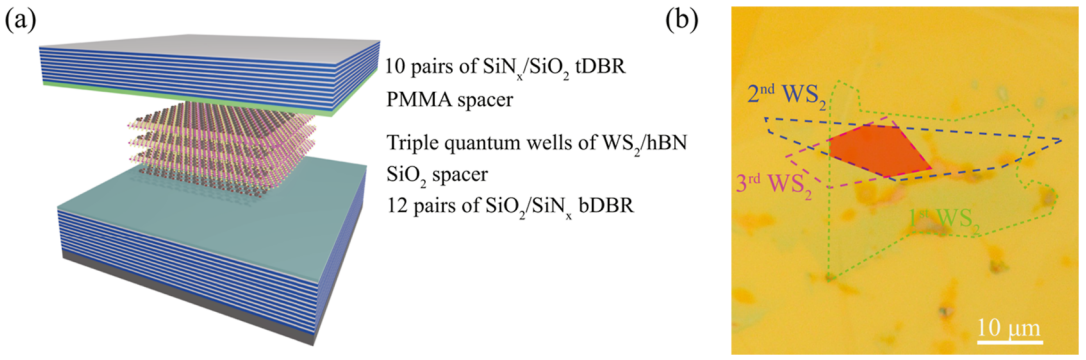

Figure 1. (a) Illustration of the device. (b) Optical microscope image of the homostructure sample inside the cavity. The dashed lines circle each monolayer WS_2, and the red area is the area of overlap of the three monolayers of WS_2.

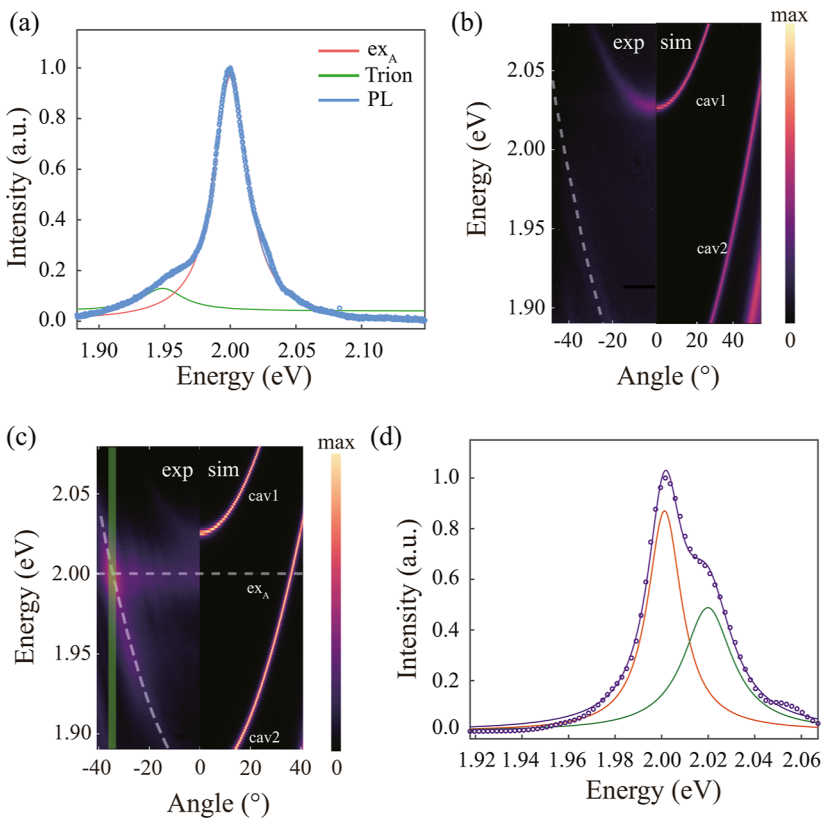

Figure 2. (a) Typical low-temperature PL of WS_2 from a monolayer region. (b) Left panel: angle-resolved PL spectrum of the bare cavity. The dashed line is the fitted energies of the uncoupled second cavity mode. Right panel: simulated reflectivity spectrum using the transfer matrix method. (c) Left panel: angle-resolved PL for the three-layer homostructure at a pump power below the threshold (19 nW/μm^2). Right panel: simulated reflectivity spectrum using the transfer matrix method. (d) Integrated PL spectrum corresponding to the gray area in Figure 2c, fit to two Lorentzian peaks. The splitting deduced from the fits is 18 ± 10 meV. All measurements were performed at 4 K.

emission and can eventually lead to the ability to control gain properties through external means such as electrostatic gating and current injection for electrically pumped operation. The laser operates in the visible regime and achieves continuous-wave single-mode operation, exhibiting an impressively bright emission with a modest optical pumping threshold of 59 nW/μm^2 at 4 K, similar to quantum-dot lasers.[34] At higher temperatures (around 200 K), the laser becomes multimode.

DEVICE DESIGN, FABRICATION, AND CHARACTERIZATION

As shown in Figure 1a, the complete sample structure includes a bottom mirror made from a distributed Bragg reflector (DBR) consisting of 12 layers of SiO_2/SiN_x, which was fabricated by using the plasma-enhanced chemical vapor deposition (PECVD) method, plus a 66 nm SiO_2 spacer layer. On this base, a superlattice of seven layers of WS_2/hBN was transferred using a top-down dry transfer technique.[35] This distinctive homostructure contains three layers of monolayer WS_2 and four 6 nm hBN spacer layers; the extra layers amplify the oscillator strength of the exciton coupling to the cavity photon mode.

Following this, a layer of poly(methyl methacrylate) (PMMA) with a thickness of 67 nm was evenly spin-coated onto the homostructure. This intermediate layer serves to align the cavity modes near the exciton energy with a designed cavity Q of 485. The microscopic image depicted in Figure 1b shows

https://doi.org/10.1021/acsphotonics.4c00549
ACS Photonics 2024, 11, 2722−2728

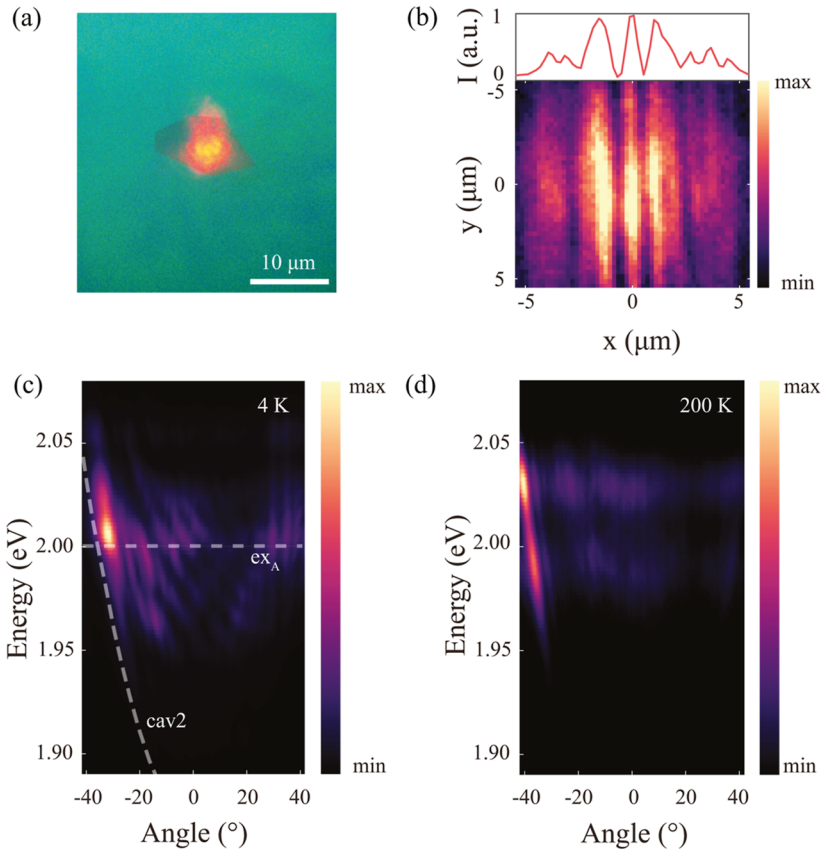

Figure 3. (a) Real-space image of the emission from the homostructure area (highlighted in the red region). The laser spot size was approximately 1 μm in radius. (b) Typical interferogram for the real-space PL spectra from the homostructure area, taken at a pump power of 1.5 P_{th}, above the lasing threshold. (c,d) Angle-resolved PL of the exciton-polariton laser measured at bath temperatures of 4 and 200 K, respectively (the effective temperature of the low temperature data may be higher than that of the bath due to inefficient cooling).

the monolayer WS_2 and the overlapping area of the three WS_2 layers, which is approximately 8 × 12 μm^2 in size. The fabrication process was concluded by placing a 10-pair distributed Bragg reflector on top using plasma-enhanced chemical vapor deposition (PECVD). This method is commonly used in many similar studies, and PMMA will protect the monolayer from degradation.[30,36,37]

We excited the sample by utilizing a 532 nm continuous diode laser with a laser spot radius of about 1.5 μm. We made measurements for the real-space photoluminescence (PL) within a monolayer domain, as depicted in Figure 2a, which presents typical PL for monolayer WS_2 post-transfer on the bottom DBR. By applying a double Lorentzian fit analysis to the spectrum, we were able to ascertain the energies of the exciton and the trion to be approximately 2.0 and 1.94 eV, respectively, consistent with the findings from our earlier studies. We then performed Fourier-plane spectroscopy, which gives the in-plane momentum dependence. The angle of emission directly corresponds to the in-plane momentum ($k_{\parallel}$) via the equation $k_{\parallel}=(\omega/c)$ (sin θ), where c is the speed of light. Multiple cavity modes were observed in both the simulation and the PL spectrum of the bare cavity (Figure 2b). Although the PL in the bare cavity is very weak, it is nonzero due to emission from impurity states in the medium. The modes in the observed spectral range correspond to 2.02 and 1.83 eV at $k_{\parallel}$ = 0.

When we moved the pump laser to the overlapping area of the three-layered WS_2 region inside the cavity, we identified an anticrossing-like feature. From the data of Figure 2c,d, a splitting of 18 ± 10 meV is observable. Since the splitting is not large compared to the line width, the coupling is not technically in the strong coupling limit. This phenomenon of weakly coupled polaritons was observed extensively within the overlap area of the three WS_2 layers. To further confirm this, we calculated the coupled harmonic oscillator model for the mixing of the bare cavity and exciton states.[38] The dashed white lines in the right panels of Figure 2b,c give the uncoupled cavity and exciton lines for the coupling used in the simulation. The gray area in Figure 2c includes the anticrossing regime. The spatial PL spectrum shown in Figure 2d results from the intensity integration over the gray area depicted in Figure 2c. Using the experimentally measured line widths for the exciton ($\hbar\Gamma_{ex}$ = 30 meV), the cavity photon ($\hbar\Gamma_{cav}$ = 16 meV), and the Rabi splitting ($\hbar\Omega_{Rabi}$ = 18 meV), we can deduce the light−matter interaction potential via $\hbar\Omega_{Rabi} = 2\sqrt{g^2 - 1/4[(\hbar\Gamma_{ex} - \hbar\Gamma_{cav}]^2}$. The calculated value of g is about 11.4 meV at the point of anticrossing, which is consistent with the PL and reflectivity spectra. This results in $g \ll |\hbar\Gamma_{ex} + \hbar\Gamma_{cav}|/2$, which puts them in a weakly coupled polariton regime.

EXCITON-POLARITON LASING

An exceptionally bright emission becomes evident when the homostructure is excited by an adequately powerful pump, as depicted in Figure 3a. The laser signal was filtered out by using a long-pass filter. The emission from the homostructure was visible with the unaided eye.

To ascertain the characteristics of this emitted light, we measured the coherence using a Michelson interferometer. This

https://doi.org/10.1021/acsphotonics.4c00549
ACS Photonics 2024, 11, 2722−2728

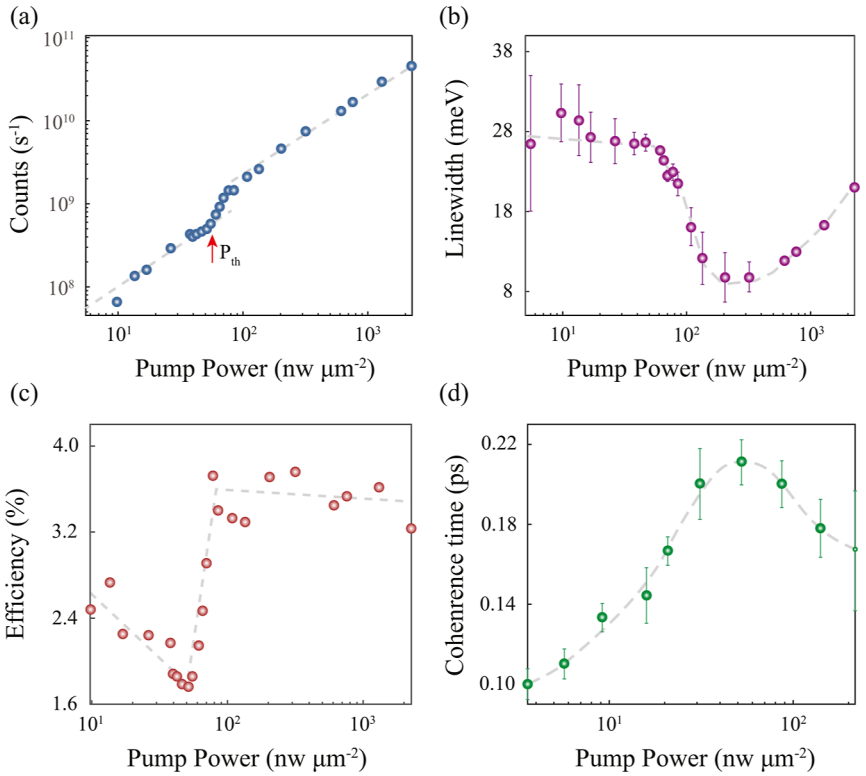

Figure 4. (a) Variation of photoluminescence (PL) photon emission with pump power. The two dashed lines show a linear relationship, and the red arrow denotes the P_{th}. (b) Relationship between polariton laser line width and pump power. (c) Efficiency of the polariton laser as a function of pump power. (d) Coherence time of the laser compared to the pump power. The dashed lines in (b−d) are guides to the eye. All measurements were performed with a bath temperature of 4 K.

setup included using a right-angle prism and a retro-mirror to flip one of the incoming images along one axis relative to the other, aligning it with the spectrometer's slit direction, defined as the x-axis. Figure 3b shows a characteristic interferogram captured under threshold conditions without any temporal delay between the two beams. The interference is discernible across the beam's dimension, ranging from −2.5 to 2.5 μm.

Switching a lens allowed us to convert real-space imaging into k-space photoluminescence imaging. The k-space PL spectrum revealed a peak emission at 615 nm, at an angle of −30° where the exciton and the second photon cavity mode intersect. As the particle density was ramped up, polaritons reached a steady state, forming a nonequilibrium Bose−Einstein condensate (BEC) in the crossing region of the photon and the exciton, as shown in Figure 3c. The interference pattern displayed in Figure 3b shows the coherence of this nonequilibrium BEC state, consistent with the well-known property of polariton condensates of emitting coherent light.[39]

Further examination of the k-space PL data revealed that the pronounced bright spot was displaced from the $k_{||} = 0$ axis. This displacement is likely because the strongest light−matter coupling is at that point; that is, the exciton and photon energies are resonant there. Polaritons that decrease in energy will have a much less excitonic nature and, therefore, less gain due to particle interactions. This is a type of polariton bottleneck effect in which the polaritons cannot thermalize into lower energy states as they descend along the lower polariton branch (LPB). As the polaritons descend along their dispersion curve, this diminishes exciton−phonon scattering efficiency, as detailed in ref 40. Additionally, an asymmetric lasing mode was observed in the momentum space. The disparity in emission angles suggests the existence of competing lasing modes, likely due to two laser transitions engaging in competition mediated by an optical phonon transition.[41] The laser maintains functionality at temperatures as high as 200 K, as shown in Figure 3d. However, at this elevated temperature, the laser's performance substantially degrades, devolving into a multimode emission.

We measured the power dependence of the light output as we varied the pump power level. The absolute light output of the polariton laser was calibrated by first sending a laser source with known power through our optical system to measure the count rate per photon of the CCD (charge-coupled device) camera. This allowed us to convert the intensity measurements captured by the CCD camera into photon counts per second.

Below the threshold for lasing, there is a direct linear relationship between the photon output and the pump power. Once the threshold power of 59 nW/μm^2 is exceeded, there was a jump in the photon output, as shown in Figure 4a. Additionally, the PL line width narrowed at the same threshold power, as indicated in Figure 4b. Higher pumping of the sample revealed a return to a linear correlation between the photon count and the pump power. Continuing to increase the pump power led to the line width broadening again, which can be understood as a consequence of increased interactions among the particles.[42]

Figure 4c depicts the efficiency of emitted light, which is measured to be around 3.82% immediately beyond the pump threshold, and this efficiency level remains consistent thereafter. This efficiency is calculated as the total photon output per second measured by the CCD camera divided by the total photon input per second from the pump laser, having corrected for the reflectivity of the top mirror and accounting for

https://doi.org/10.1021/acsphotonics.4c00549
ACS Photonics 2024, 11, 2722−2728

unobserved transmission output through the bottom mirror, knowing its transmission at the emission wavelength (for more details about the calculation, refer to the Supporting Information). The lasing threshold of our structure is considerably lower than that of quantum-dot lasers, which usually exhibit a minimum threshold of approximately 500 nW/μm^2,[43,44] and comparable to that of other polariton lasers, as discussed in the Introduction. A fit to the standard laser equation is given in the Supporting Information.

To study the temporal coherence characteristic of polariton lasing, we varied the length of one of the arms of the Michelson interferometer and determined the coherence time as a function of the pump power. The experimental visibility data is quantified as the ratio between the difference in the intensity of the maximum and the minimum to their sum, formulated as $(I_{max} - I_{min})/(I_{max} + I_{min})$. For each pump power, we fitted the collected visibility data with a Gaussian function to ascertain the coherence time. Figure 4d shows the coherence time versus pump power (note that the horizontal axis for power is a smaller range than in the other data of Figure 4). We observed that the coherence time increased from 100 to 211 fs when the pump power exceeded the lasing threshold.

CONCLUSIONS

All of the power-dependent measurements are consistent with the interpretation that we have observed lasing with a pronounced emission at 615 nm. The power series analysis indicates that the lasing threshold was 59 nW/μm^2 injected pump power (uncorrected for reflection from the top mirror), which corresponds to an injected carrier density of the order of 10^8 cm^{-2}, assuming a cavity lifetime of 5 ps, based on the Q of the cavity and the cavity mode spacing. Remarkably, even with its extremely low threshold, the system maintained a high efficiency level, reaching around 3.82% of injected electron−hole pairs turning into photons in the laser output. The polariton effect is seen to be playing a role in that the emission occurs in the region of exciton-photon resonance, where the polariton effect is strongest. The lasing action maintains its intensity even at raised temperatures. However, at high temperatures, it becomes multimode. Despite this, the prospects are good for realizing a room-temperature, micrometer-sized, ultralow threshold and efficient lasing using two-dimensional materials.

ASSOCIATED CONTENT

Supporting Information

The Supporting Information is available free of charge at https://pubs.acs.org/doi/10.1021/acsphotonics.4c00549.

Calculation for the slope efficiency calibration and the rate equation of the exciton-polariton laser; simulation for the reflectivity of the DBRs used in the sample; laser emission from the positive angle; and temperature-dependent PL for a monolayer WS_2 fitted with the Varshni formula (PDF)

AUTHOR INFORMATION

Corresponding Authors

Jian Wu − *State Key Laboratory of Precision Spectroscopy, East China Normal University, Shanghai 200241, China; Collaborative Innovation Center of Extreme Optics, Taiyuan, Shanxi 030006, China; Chongqing Key Laboratory of Precision Optics, Chongqing 401121, China;* orcid.org/0000-0002-1318-2291; Email: jwu@phy.ecnu.edu.cn

Zheng Sun − *State Key Laboratory of Precision Spectroscopy, East China Normal University, Shanghai 200241, China; Collaborative Innovation Center of Extreme Optics, Taiyuan, Shanxi 030006, China;* orcid.org/0000-0002-5209-2563; Email: zsun@lps.ecnu.edu.cn

David Snoke − *Department of Physics and Astronomy, University of Pittsburgh, Pittsburgh, Pennsylvania 15260, United States*; Phone: +86-18017854698; Email: snoke@pitt.edu

Authors

Yuening Fan − *State Key Laboratory of Precision Spectroscopy, East China Normal University, Shanghai 200241, China*

Qiaochu Wan − *Department of Physics and Astronomy, University of Pittsburgh, Pittsburgh, Pennsylvania 15260, United States*

Qi Yao − *Department of Physics and Astronomy, University of Pittsburgh, Pittsburgh, Pennsylvania 15260, United States*

Xingzhou Chen − *State Key Laboratory of Precision Spectroscopy, East China Normal University, Shanghai 200241, China*

Yuanjun Guan − *State Key Laboratory of Precision Spectroscopy, East China Normal University, Shanghai 200241, China*

Hassan Alnatah − *Department of Physics and Astronomy, University of Pittsburgh, Pittsburgh, Pennsylvania 15260, United States*

Daniel Vaz − *Department of Physics and Astronomy, University of Pittsburgh, Pittsburgh, Pennsylvania 15260, United States*

Jonathan Beaumariage − *Department of Physics and Astronomy, University of Pittsburgh, Pittsburgh, Pennsylvania 15260, United States*

Kenji Watanabe − *Research Center for Electronic and Optical Materials, Tsukuba 305-0044, Japan;* orcid.org/0000-0003-3701-8119

Takashi Taniguchi − *Research Center for Materials Nanoarchitectonics, Tsukuba 305-0044, Japan;* orcid.org/0000-0002-1467-3105

Complete contact information is available at: https://pubs.acs.org/10.1021/acsphotonics.4c00549

Author Contributions

[¶]Y.F. and Q.W. contributed equally to this work. Z.S., D.S., and J.W. supervised the project. Y.F., Q.W., Q.Y., X.C., Y.G., H.A., D.V., J.B., D.S., and Z.S. fabricated the full samples, performed the optical measurements, and analyzed the data. All the authors contributed to the discussion of the results and the writing of the manuscript.

Funding

The work was supported by the National Key Research and Development Program of China (2021YFA1200803), the National Natural Science Foundation of China (12174111), and the Science and Technology Commission of Shanghai Municipality (23JC1402000). D.S., Q.W., H.A., Q.Y., and J.B. acknowledge support from the U.S. National Science Foundation (DMR-2004570) and MURI (W911NF-17−1−0312). K.W. and T.T. acknowledge support from the JSPS KAKENHI (grant numbers 20H00354 and 23H02052) and the World Premier International Research Center Initiative (WPI), MEXT, Japan.

Notes

The authors declare no competing financial interest.

REFERENCES

(1) Wu, S.; Buckley, S.; Schaibley, J. R.; Feng, L.; Yan, J.; Mandrus, D. G.; Hatami, F.; Yao, W.; Vučković, J.; Majumdar, A.; et al. Monolayer semiconductor nanocavity lasers with ultralow thresholds. *Nature* **2015**, *520*, 69−72.

(2) Ye, Y.; Wong, Z. J.; Lu, X.; Ni, X.; Zhu, H.; Chen, X.; Wang, Y.; Zhang, X. Monolayer excitonic laser. *Nat. Photonics* **2015**, *9*, 733−737.

(3) Li, Y.; Zhang, J.; Huang, D.; Sun, H.; Fan, F.; Feng, J.; Wang, Z.; Ning, C.-Z. Room-temperature continuous-wave lasing from monolayer molybdenum ditelluride integrated with a silicon nanobeam cavity. *Nat. Nanotechnol.* **2017**, *12*, 987−992.

(4) Shang, J.; Cong, C.; Wang, Z.; Peimyoo, N.; Wu, L.; Zou, C.; Chen, Y.; Chin, X. Y.; Wang, J.; Soci, C.; Huang, W.; Yu, T. Room-temperature 2D semiconductor activated vertical-cavity surface-emitting lasers. *Nat. Commun.* **2017**, *8*, 543.

(5) Splendiani, A.; Sun, L.; Zhang, Y.; Li, T.; Kim, J.; Chim, C. Y.; Galli, G.; Wang, F. Emerging photoluminescence in monolayer MoS_2. *Nano Lett.* **2010**, *10*, 1271−1275.

(6) Liu, X.; Galfsky, T.; Sun, Z.; Xia, F.; Lin, E.-C.; Lee, Y.-H.; Kéna-Cohen, S.; Menon, V. M. Strong light-matter coupling in two-dimensional atomic crystals. *Nat. Photonics* **2015**, *9*, 30−34.

(7) Anton-Solanas, C.; Waldherr, M.; Klaas, M.; Suchomel, H.; Harder, T. H.; Cai, H.; Sedov, E.; Klembt, S.; Kavokin, A. V.; Tongay, S.; Watanabe, K.; Taniguchi, T.; Höfling, S.; Schneider, C. Bosonic condensation of exciton−polaritons in an atomically thin crystal. *Nat. Mater.* **2021**, *20*, 1233−1239.

(8) Chen, X.; Alnatah, H.; Mao, D.; Xu, M.; Fan, Y.; Wan, Q.; Beaumariage, J.; Xie, W.; Xu, H.; Shi, Z. Y.; Snoke, D.; Sun, Z.; Wu, J. Bose Condensation of Upper-Branch Exciton-Polaritons in a Transferable Microcavity. *Nano Lett.* **2023**, *23*, 9538−9546.

(9) Deng, H.; Haug, H.; Yamamoto, Y. Exciton-polariton bose-einstein condensation. *Rev. Mod. Phys.* **2010**, *82*, 1489−1537.

(10) Snoke, D. *Solid State Physics: Essential Concepts*, 2nd ed.; Cambridge University Press, 2020; pp 618−686.

(11) Ardizzone, V.; De Marco, L.; De Giorgi, M.; Dominici, L.; Ballarini, D.; Sanvitto, D. Emerging 2D materials for room-temperature polaritonics. *Nanophotonics* **2019**, *8*, 1547−1558.

(12) Klaas, M.; Flayac, H.; Amthor, M.; Savenko, I.; Brodbeck, S.; Ala-Nissila, T.; Klembt, S.; Schneider, C.; Höfling, S. Evolution of temporal coherence in confined exciton-polariton condensates. *Phys. Rev. Lett.* **2018**, *120*, 017401.

(13) Kasprzak, J.; Richard, M.; Baas, A.; Deveaud, B.; André, R.; Poizat, J.-P.; Dang, L. S. Second-order time correlations within a polariton Bose−Einstein condensate in a CdTe microcavity. *Phys. Rev. Lett.* **2008**, *100*, 067402.

(14) Tsintzos, S.; Pelekanos, N.; Konstantinidis, G.; Hatzopoulos, Z.; Savvidis, P. A GaAs polariton light-emitting diode operating near room temperature. *Nature* **2008**, *453*, 372−375.

(15) Li, F.; Orosz, L.; Kamoun, O.; Bouchoule, S.; Brimont, C.; Disseix, P.; Guillet, T.; Lafosse, X.; Leroux, M.; Leymarie, J.; et al. Fabrication and characterization of a room-temperature ZnO polariton laser. *Appl. Phys. Lett.* **2013**, *102*, 191118.

(16) Paschos, G.; Somaschi, N.; Tsintzos, S. I.; Coles, D.; Bricks, J. L.; Hatzopoulos, Z.; Lidzey, D.; Lagoudakis, P. G.; Savvidis, P. G. Hybrid organic-inorganic polariton laser. *Sci. Rep.* **2017**, *7*, 11377.

(17) Su, R.; Diederichs, C.; Wang, J.; Liew, T. C.; Zhao, J.; Liu, S.; Xu, W.; Chen, Z.; Xiong, Q. Room-temperature polariton lasing in all-inorganic perovskite nanoplatelets. *Nano Lett.* **2017**, *17*, 3982−3988.

(18) Zhu, W.; Xu, T.; Wang, H.; Zhang, C.; Deotare, P. B.; Agrawal, A.; Lezec, H. J. Surface plasmon polariton laser based on a metallic trench Fabry-Perot resonator. *Sci. Adv.* **2017**, *3*, No. e1700909.

(19) Basov, D.; Fogler, M.; García de Abajo, F. J. Polaritons in van der Waals materials. *Science* **2016**, *354*, aag1992.

(20) Chaves, A.; Azadani, J. G.; Alsalman, H.; da Costa, D. R.; Frisenda, R.; Chaves, A. J.; Song, S. H.; Kim, Y. D.; He, D.; Zhou, J.; Castellanos-Gomez, A.; Peeters, F. M.; Liu, Z.; Hinkle, C. L.; Oh, S. H.; Ye, P. D.; Koester, S. J.; Lee, Y. H.; Avouris, P.; Wang, X.; Low, T. Bandgap engineering of two-dimensional semiconductor materials. *npj 2D Mater. Appl.* **2020**, *4*, 29.

(21) Maiti, R.; Hemnani, R. A.; Amin, R.; Ma, Z.; Tahersima, M. H.; Empante, T. A.; Dalir, H.; Agarwal, R.; Bartels, L.; Sorger, V. J. A semi-empirical integrated microring cavity approach for 2D material optical index identification at 1.55 μm. *Nanophotonics* **2019**, *8*, 435−441.

(22) Salehzadeh, O.; Djavid, M.; Tran, N. H.; Shih, I.; Mi, Z. Optically pumped two-dimensional MoS_2 lasers operating at room-temperature. *Nano Lett.* **2015**, *15*, 5302−5306.

(23) Galfsky, T.; Sun, Z.; Considine, C. R.; Chou, C. T.; Ko, W. C.; Lee, Y. H.; Narimanov, E. E.; Menon, V. M. Broadband Enhancement of Spontaneous Emission in Two-Dimensional Semiconductors Using Photonic Hypercrystals. *Nano Lett.* **2016**, *16*, 4940−4945.

(24) Zhang, L.; Zhang, Z.; Wu, F.; Wang, D.; Gogna, R.; Hou, S.; Watanabe, K.; Taniguchi, T.; Kulkarni, K.; Kuo, T.; et al. Twist-angle dependence of moiré excitons in $WS_2/MoSe_2$ heterobilayers. *Nat. Commun.* **2020**, *11*, 5888.

(25) Sun, Z.; Beaumariage, J.; Xu, K.; Liang, J.; Hou, S.; Forrest, S. R.; Fullerton-Shirey, S. K.; Snoke, D. W. Electric-field-induced optical hysteresis in single-layer WSe_2. *Appl. Phys. Lett.* **2019**, *115*, 161103.

(26) Sun, Z.; Xu, K.; Liu, C.; Beaumariage, J.; Liang, J.; Fullerton-Shirey, S. K.; Shi, Z. Y.; Wu, J.; Snoke, D. Photoluminescence Switching Effect in a Two-Dimensional Atomic Crystal. *ACS Nano* **2021**, *15*, 19439−19445.

(27) Gonzalez Marin, J. F.; Unuchek, D.; Watanabe, K.; Taniguchi, T.; Kis, A. MoS2 photodetectors integrated with photonic circuits. *npj 2D Mater. Appl.* **2019**, *3*, 14.

(28) Ross, J. S.; Klement, P.; Jones, A. M.; Ghimire, N. J.; Yan, J.; Mandrus, D.; Taniguchi, T.; Watanabe, K.; Kitamura, K.; Yao, W.; et al. Electrically tunable excitonic light-emitting diodes based on monolayer WSe_2 p−n junctions. *Nat. Nanotechnol.* **2014**, *9*, 268−272.

(29) Furchi, M. M.; Pospischil, A.; Libisch, F.; Burgdorfer, J.; Mueller, T. Photovoltaic effect in an electrically tunable van der Waals heterojunction. *Nano Lett.* **2014**, *14*, 4785−4791.

(30) Zhao, J.; Su, R.; Fieramosca, A.; Zhao, W.; Du, W.; Liu, X.; Diederichs, C.; Sanvitto, D.; Liew, T. C.; Xiong, Q. Ultralow threshold polariton condensate in a monolayer semiconductor microcavity at room temperature. *Nano Lett.* **2021**, *21*, 3331−3339.

(31) Pau, S.; Björk, G.; Jacobson, J.; Cao, H.; Yamamoto, Y. Microcavity exciton-polariton splitting in the linear regime. *Phys. Rev. B* **1995**, *51*, 14437−14447.

(32) Zhao, J.; Fieramosca, A.; Dini, K.; Bao, R.; Du, W.; Su, R.; Luo, Y.; Zhao, W.; Sanvitto, D.; Liew, T. C.; et al. Exciton polariton interactions in Van der Waals superlattices at room temperature. *Nat. Commun.* **2023**, *14*, 1512.

(33) Elrafei, S. A.; Heijnen, L. M.; Godiksen, R. H.; Curto, A. G. Approaching the absorption limit with monolayer semiconductor superlattices, 2024. arXiv:2402.10179. https://doi.org/10.48550/arXiv.2402.10179.

(34) Strauf, S.; Jahnke, F. Single quantum dot nanolaser. *Laser Photonics Rev.* **2011**, *5*, 607−633.

(35) Fan, S.; Vu, Q. A.; Tran, M. D.; Adhikari, S.; Lee, Y. H. Transfer assembly for two-dimensional van der Waals heterostructures. *2D Materials* **2020**, *7*, 022005.

(36) Yun, T.; Estrecho, E.; Truscott, A. G.; Ostrovskaya, E. A.; Wurdack, M. J. Fabrication of high-quality PMMA/SiOx spaced planar microcavities for strong coupling of light with monolayer WS_2 excitons. *Appl. Phys. Lett.* **2022**, *121*, 081105.

(37) Qiu, L.; Chakraborty, C.; Dhara, S.; Vamivakas, A. Room-temperature valley coherence in a polaritonic system. *Nat. Commun.* **2019**, *10*, 1513.

(38) Snoke, D. Spontaneous Bose coherence of excitons and polaritons. *Science* **2002**, *298*, 1368−1372.

(39) Cong, C.; Shang, J.; Wang, Y.; Yu, T. Optical properties of 2D semiconductor WS_2. *Adv. Opt. Mater.* **2018**, *6*, 1700767.

(40) Tassone, F.; Piermarocchi, C.; Savona, V.; Quattropani, A.; Schwendimann, P. Bottleneck effects in the relaxation and photoluminescence of microcavity polaritons. *Phys. Rev. B* **1997**, *56*, 7554−7563.

https://doi.org/10.1021/acsphotonics.4c00549
ACS Photonics 2024, 11, 2722−2728

(41) Franz, K. J.; Menzel, S.; Hoffman, A. J.; Wasserman, D.; Cockburn, J. W.; Gmachl, C. High k-space lasing in a dual-wavelength quantum cascade laser. *Nat. Photonics* **2009**, *3*, 50−54.
(42) Deng, H.; Weihs, G.; Snoke, D.; Bloch, J.; Yamamoto, Y. Polariton lasing vs. photon lasing in a semiconductor microcavity. *Proc. Natl. Acad. Sci. U.S.A.* **2003**, *100*, 15318−15323.
(43) Zhong, H.; Yu, Y.; Zheng, Z.; Ding, Z.; Zhao, X.; Yang, J.; Wei, Y.; Chen, Y.; Yu, S. Ultra-low threshold continuous-wave quantum dot mini-BIC lasers. *Light: Sci. Appl.* **2023**, *12*, 100.
(44) Taghipour, N.; Whitworth, G. L.; Othonos, A.; Dalmases, M.; Pradhan, S.; Wang, Y.; Kumar, G.; Konstantatos, G. Low-Threshold, Highly Stable Colloidal Quantum Dot Short-Wave Infrared Laser enabled by Suppression of Trap-Assisted Auger Recombination. *Adv. Mater.* **2022**, *34*, 2107532.

https://doi.org/10.1021/acsphotonics.4c00549
ACS Photonics 2024, 11, 2722−2728